



Contents lists available at ScienceDirect

# Journal of Quantitative Spectroscopy & Radiative Transfer

journal homepage: [www.elsevier.com/locate/jqsrt](http://www.elsevier.com/locate/jqsrt)

## Photoionization of P<sup>+</sup>: Experiment and theory



S.N. Nahar<sup>a,\*</sup>, E.M. Hernández<sup>b</sup>, L. Hernández<sup>c</sup>, A. Antillón<sup>c</sup>, A. Morales-Mori<sup>c</sup>,  
O. González<sup>d</sup>, A.M. Covington<sup>e</sup>, K.C. Chartkunchand<sup>e</sup>, D. Hanstorp<sup>f</sup>,  
A.M. Juárez<sup>c</sup>, G. Hinojosa<sup>c</sup>

<sup>a</sup> The Ohio State University, OH43210-1173, USA

<sup>b</sup> Universidad Autónoma del Estado de Morelos, Cuernavaca 62209, Mexico

<sup>c</sup> Instituto de Ciencias Físicas, Universidad Nacional Autónoma de México, A. P. 48-3, Cuernavaca 62251, Mexico

<sup>d</sup> University of Groningen, 9747 AA Groningen, The Netherlands

<sup>e</sup> Physics Department, University of Nevada, Reno, NV 89557-0220, USA

<sup>f</sup> University of Gothenburg, SE-412 96 Gothenburg, Sweden

### ARTICLE INFO

#### Article history:

Received 25 June 2016

Received in revised form

17 September 2016

Accepted 19 September 2016

Available online 5 October 2016

#### Keywords:

Photoionization of P II

Experiment at ALS

Breit–Pauli R-matrix method

Autoionizing resonances

Relativistic effects at low energy

### ABSTRACT

An experimental and theoretical study of the single photoionization cross section of the P<sup>+</sup> cation of phosphorus is presented. Photoionization (PI) cross sections are instrumental for the determination of abundances in the interstellar medium. The experiment was performed by merging an ion beam with a photon beam. The photon beam was nearly monochromatic and had an energy resolution of 24 meV. Calculations were carried out using the Breit–Pauli R-matrix method. The combined study was developed in the photon energy interval from 18 eV (68.9 nm) to 50 eV (24.8 nm). Comparison between the measured and the calculated cross section shows good agreement in general and identifies features of the process and existence of states in the experimental beam. The present results should provide for more accurate modeling of P<sup>+</sup>.

© 2016 Elsevier Ltd. All rights reserved.

## 1. Introduction

The advent of third generation synchrotron radiation sources has made high-resolution experimental data available, triggering the advance of theoretical methods. Photoionization (PI) cross sections are instrumental for the determination of abundances in the interstellar medium. Phosphorus is of particular interest because its relative abundance is used as an indicator of possible life-propitious regions in the Universe [1]. It is an important element of RNAs existing in all living tissues. Lines of P II and P III have been found in the high resolution spectra of hot OB stars under the project called ASTRO-2 (J. Hillier, private communication, 2015).

From a theoretical point of view, P<sup>+</sup> is interesting because it has a silicon-like electronic configuration and is also an intermediate-sized near neutral ion in which electron–electron correlation is expected to be large. To our knowledge, PI cross sections of the single ionized cation of phosphorus are not available in literature.

Earlier studies of the photoionization cross sections of Si I isoelectronic sequence were obtained under the opacity project (OP) [2] by Mendoza and Zeppen [3], Nahar and Pradhan [4], and Nahar [5] using the close coupling approximation and the R-matrix method. In these isoelectronic sequence calculations, the PI of P<sup>+</sup> was not considered.

In this study we present a state-of-the-art theoretical calculation derived from the Breit–Pauli R-matrix (BPRM) method and cutting-edge experimental data for the single PI of P<sup>+</sup>.

\* Corresponding author.

E-mail address: [nahar.1@osu.edu](mailto:nahar.1@osu.edu) (S.N. Nahar).

## 2. Experiment

The experimental data were measured using the Ion Photon Beam end station on undulator beam line 10.0.1.2 of the Advanced Light Source (ALS) at the Lawrence Berkeley National Laboratory. The method was based on the merged-beams technique [6] and has been described previously in detail by Covington et al. [7]. A more recent description of the experimental method was given by Müller et al. [8]. A general description of the present experiment with details relevant to the present investigation will be given here.

The fundamental idea of this technique consists of merging a photon-beam and an ion-beam over a common collinear path. As a result of the beams interaction along the overlapping zone,  $P^+$  ions from the initial ion beam may be photoionized yielding doubly charged  $P^{2+}$  ions. The resulting doubly charged ions are separated from the parent ion beam and relevant parameters of both beams such as their intensities and form factors were measured.

The photons required to photoionize  $P^+$  cations were generated by making the storage ring electrons oscillate within a 10-cm period undulator positioned in the 0.5 A constant current, 1.9 GeV synchrotron ring. A resulting highly collimated photon beam of spatial width less than 1.5 mm and divergence less than  $0.06^\circ$  was produced. The photon beam was further monochromatized with a spherical grating. This grating was configured in the grazing incidence mode that allowed for selection of the photon energy with a controlled grating rotation and with translation of the exit slit of the monochromator. At the same time, the undulator gap was adjusted to maximize the photon beam intensity.

The background  $P^{2+}$  ions produced by collisional induced ionization were subtracted from the photo-ion signal by intermittently cutting the photon beam with a chopping-wheel. A partial photon energy error of  $\pm 10$  meV was achieved by calibrating the photon energy in a side-branch gas-cell using photon ionization energies of He [9] and Kr [10] in an energy range from 21.218 eV to 63.355 eV.

The ion beam was produced by injecting a mixture of  $PF_3$  and Ar gases into an ECR ion source. The  $P^+$  ion beam was selected by its mass-to-charge ratio by a  $60^\circ$  sector magnet located after the all-permanent-magnet ECR ion source. A typical  $P^+$  ion beam current was 350 nA.

The ion beam was then steered through a  $90^\circ$  electrostatic spherical-sector bending-plates setup that merged the ion beam with the photon-beam. Following, in the beams trajectory, a voltage biased cylindrical-mesh was used to define the length of the beams interaction. The photo-ions that are formed inside this interaction region (IR) were separated from those produced along the rest because the bias voltage applied to the IR energy-marked the  $P^{2+}$  ions generated inside it. The overlap between the ion and photon beams was measured with the help of mechanically controlled two-dimensional slit scanners which produce profiles of both ion and photon beams. These profiles were used to calculate the overlap between the photon and ion beams, thereby allowing us to derive the interaction volume needed for the absolute cross sections computation. A  $45^\circ$  dipole analyzing magnet de-

merged the beams separating the  $P^{2+}$  products from the parent  $P^+$  beam. The de-merging magnetic field was selected such that only the  $P^{2+}$  product photo-ions generated inside the IR were collected.

The single absolute PI cross section  $\sigma_{PI}$  of  $P^+$  was derived from

$$\sigma_{PI} = \frac{Rqe^2 v_i \epsilon}{I^+ I' \int F(\xi) d\xi} \quad (1)$$

where  $R$  is the photoion signal count rate,  $q$  is the charge state of the parent ion,  $e = 1.6 \times 10^{-19}$  C,  $v_i$  is the ion beam velocity in  $\text{cm s}^{-1}$ ,  $\epsilon$  is the responsivity of the photodiode,  $I^+$  is the ion beam current (A) and  $I'$  is the photodiode current (A).  $\xi$  is the ion beam propagation direction and  $\int F(\xi) d\xi$  is the form factor  $F(\xi)$  integrated along the IR length.  $F(\xi)$  was measured by the mechanical beam profilers in the entrance, center and output ( $i = 1, 2, 3$  respectively) of the IR. These three values of  $F(\xi_i)$  were determined from

$$F(\xi_i) = \frac{\iint I^+(x, y) I'(x, y) dx dy}{\iint I^+(x, y) dx dy \iint I'(x, y) dx dy} \quad (2)$$

where  $I^+(x, y)$  and  $I'(x, y)$  correspond to the ion and photon beam profiles that define at each location the spatial overlap of the beams along the common IR path. To derive the integral of Eq. (1),  $F(\xi)$  was interpolated within the IR total length and integrated over  $\xi$ .

Figs. 1 and 3 show total spectra that were measured in scans of one-electron-volt intervals, these individual sections of spectrum will be called, from here on, 1 eV-scans. The intensity in these scans consists of ion-yield normalized to photon and ion intensities as a function of the photon energy. During the experiment, each 1 eV-scan was overlapped 0.5 eV with the following scan. This reduced the possible effects from a slight mechanical backlash from the monochromators and also improved the automatic photon flux optimization adjustments in the photon beam line. The 1 eV-scans were combined by normalizing the intensities. The total resulting spectrum was then normalized to the cross section measurements performed at specific energy values (shown in Table 2).

The gluing routine implied arbitrarily choosing one 1 eV-scan and shift the neighboring scans by  $\pm 1$  meV to match structures. To estimate the error introduced by this method of gluing, the computing routine was executed several times with different initial 1 eV-scans, yielding an estimated error in the photon energy of  $\pm 8$  meV. This error source combined with the gas-cell energy calibration uncertainty of  $\pm 10$  meV yields a total overall uncertainty of  $\pm 13$  meV in the photon energy.

The most important sources of systematic errors in the absolute cross section measurements are the beams overlap integral, the photodiode responsivity and the photodiode current measurement. For this experiment, we estimated a larger error for the photodiode current measurement of 10% in instead of 3% given in Covington et al. [7] where other contributions to the total systematic uncertainty are listed. For this experiment, a total systematic error of 20% in the cross section absolute measurements is given.

The cross section measurements can be underestimated due to the presence of higher-order radiation in the photon beam. This effect is specially large at the lower energy regime of the present measurements. The same experimental setup was used to study the photoionization of  $W^+$  by Müller et al. [8]. They derived a correction function for this particular experiment and found that the correction to the cross section at 20 eV was almost 40% and at 25 eV was on the order of 17%. To account for this effect, we performed an approximation to this correction by interpolating from correction factors of 1.9 at 16 eV, 1.4 at 20 eV and 1.17 at 25 eV. Assuming a monotonic decay of the correction function and based on the fact that above 25 eV, the correction function is lower than the systematic error of the cross section, we arbitrarily added 1 at 35 eV for the correction function. We used this approximation for  $f_c$  to offer a correction in the energy range from 18 eV to 35 eV of the present data. It is important to point out that an additional uncertainty of 50% of the difference between the measured and the higher-order-radiation corrected cross sections has to be applied. These error bars are shown in Fig. 1.

### 3. Theory

Autoionizing states introduce resonances in the PI process. Theoretically, resonances can be generated naturally in any ab initio calculation by including core excitations in the wave function, as considered in the close coupling (CC) approximation. In the CC approximation the atomic system is represented by a  $(N+1)$  number of electrons where the core ion is an  $N$ -electrons system interacting with the  $(N+1)$ th electron. The  $(N+1)$ th electron is bound or in the continuum depending on its negative or positive energy ( $E$ ). The total wave function,  $\Psi_E$ , in a symmetry  $SL\pi$  is expressed by an expansion as (e.g., [11])

$$\Psi_E(e^- + ion) = A \sum_i \chi_i(ion) \theta_i + \sum_j c_j \Phi_j \quad (3)$$

where the core ion eigenfunction,  $\chi_i$ , represents ground and various excited states. The sum is over the number of states considered. The core is coupled with the  $(N+1)$ th electron function,  $\theta_i$ . The  $(N+1)$ th electron with kinetic energy  $k_i^2$  is in a channel labeled as  $S_i L_i \pi_i k_i^2 \ell_i (SL\pi)$ .  $A$  is the antisymmetrization operator. In the second sum, the  $\Phi_j$ s are bound channel functions of the  $(N+1)$ -electrons system that provides the orthogonality between the continuum and the bound electron orbitals and accounts for short range correlation. Substitution of  $\Psi_E(e^- + ion)$  in the Schrödinger equation

$$H_{N+1} \Psi_E = E \Psi_E \quad (4)$$

introduces a set of coupled equations that are solved using the  $R$ -matrix approach.

The details of the  $R$ -matrix method in the CC approximation can be found in, e.g., [11–15]. The relativistic effects are included through Breit–Pauli approximation

(e.g., [11]), where the Hamiltonian is given by

$$H_{N+1}^{BP} = \sum_{i=1}^{N+1} \left\{ -\nabla_i^2 - \frac{2Z}{r_i} + \sum_{j>i}^{N+1} \frac{2}{r_{ij}} \right\} + H_{N+1}^{mass} + H_{N+1}^{Dar} + H_{N+1}^{so} \quad (5)$$

in Rydberg unit. The relativistic correction terms are corrected by mass,  $H^{mass} = -\frac{\alpha^2}{4} \sum_i p_i^4$ , Darwin,  $H^{Dar} = \frac{Z\alpha^2}{4} \sum_i \nabla^2 \left( \frac{1}{r_i} \right)$ , and spin-orbit interaction,  $H^{so} = Z\alpha^2 \sum_i \frac{1}{r_i^3} \mathbf{l}_i \cdot \mathbf{s}_i$ .  $R$ -matrix Breit–Pauli (BPRM) approximation also includes part of two-body interaction terms, such as the ones without the momentum operators [11]. In this approximation the set of  $SL\pi$  is recoupled for  $J\pi$  levels of  $(e^- + ion)$  system which is followed by diagonalization of the Hamiltonian.

The solution of BRPM approximation is a continuum wave function,  $\Psi_F$ , for an electron with positive energies ( $E > 0$ ), or a bound state,  $\Psi_B$ , at a negative total energy ( $E \leq 0$ ). The complex resonant structures in photoionization are produced from channel couplings between continuum channels that are open ( $k_i^2 > 0$ ), and ones that are closed ( $k_i^2 < 0$ ), at electron energies  $k_i^2$  corresponding to autoionizing states of the Rydberg series,  $S_i L_i j_i \pi_i \nu \ell$ .  $\nu$  is the effective quantum number of the states in the series converging on to the excited core thresholds.

The photoionization cross section ( $\sigma_{PI}$ ) is given by (e.g., [11])

$$\sigma_{PI} = \frac{4\pi^2}{3c} \frac{1}{g_i} \omega \mathbf{S} \quad (6)$$

where  $g_i$  is the statistical weight factor of the bound state,  $\omega$  is the incident photon energy and  $\mathbf{S}$  is the generalized line strength

$$\mathbf{S} = | \langle \Psi_f \| \mathbf{D}_L \| \Psi_i \rangle |^2 = \left| \left\langle \Psi_f \left| \sum_{j=1}^{N+1} r_j \right| \Psi_i \right\rangle \right|^2, \quad (7)$$

where  $\Psi_i$  and  $\Psi_f$  are the initial and final state wave functions and  $\mathbf{D}_L$  is the dipole operator in length form.

### 4. Computation

BPRM calculations are initiated through a package of codes [15–17] for various stages with the wave function of the core as the initial input. The core wave function was obtained from atomic structure calculations using code SUPERSTRUCTURE (SS) [18,19]. SS uses Thomas–Fermi–Dirac–Amaldi potential and includes relativistic contributions in Breit–Pauli approximation. Table 1 presents 18, the ground and 17 excited, fine structure levels of  $P^{2+}$  included in the wave function expansion of  $P^+$ . They were obtained from optimization of 19 configurations up to 5s orbital of  $P^{2+}$ . The calculated energies from SS are compared with observed values (listed at NIST [20] compilation) in Table 1. Comparison shows agreement between SS and observed values within a few percent.

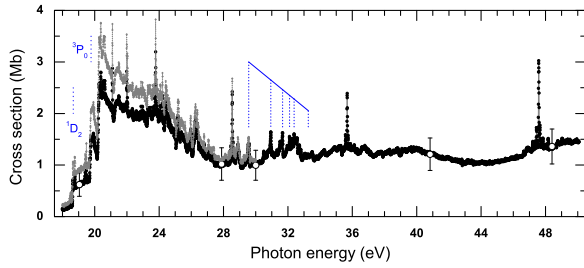


**Fig. 1.** Total photoionization cross section,  $\sigma_{PI}$ , of  $P^+$  measured with a photon energy resolution of 24 meV: black dots joined with gray lines. Open circles represent the absolute cross section measurements of Table 2. A portion of the spectrum was multiplied by a correction factor  $f_c$  for higher-order radiation population in the photon beam: gray dots joined with gray lines. An additional uncertainty of 50% of the difference between the corrected and uncorrected cross section has to be included for the corrected portion of  $\sigma_{PI}$ . In the case of the absolute data point at 19.05 eV, the total error associated to the correction is 0.27, this error is not plotted. The thresholds of two lower lying levels of  $P^+$  were positioned at NIST energies and are labeled with their corresponding terms:  $^1D_2$  and  $^3P_0$ . Some resonant structures are marked by vertical lines grouped by a sloped line. These structures may resemble a Rydberg series that seems to converge to  $(3s3p^2)^2P_{1/2}$  final state of  $P^{2+}$ ; however, is not well resolved and its assignment is uncertain. The peaks indicated by vertical lines are: 29.551 eV, 30.934 eV, 31.661 eV, 32.105 eV and 32.385 eV.

**Table 1**

Levels and energies ( $E_t$ ) of core ion  $P^{2+}$  in wave function expansion of  $P^+$ .

Level	$J_t$	$E_t$ (Ry) NIST	$E_t$ (Ry) SS	
1	$3s^23p(^2P^o)$	1/2	0	0
2	$3s^23p(^2P^o)$	3/2	0.005095	0.0043
3	$3s3p^2(^4P)$	5/2	0.511829	0.5128
4	$3s3p^2(^4P)$	3/2	0.520570	0.5103
5	$3s3p^2(^4P)$	1/2	0.518708	0.5087
6	$3s3p^2(^2D)$	3/2	0.682693	0.7055
7	$3s3p^2(^2D)$	5/2	0.682957	0.7056
8	$3s3p^2(^2S)$	1/2	0.993620	0.9941
9	$3s3p^2(^2P)$	1/2	0.993620	1.0334
10	$3s3p^2(^2P)$	3/2	0.997044	1.0361
11	$3s^23d(^2D)$	3/2	1.065039	1.1438
12	$3s^23d(^2D)$	5/2	1.065142	1.1439
13	$3s^24s(^2S)$	1/2	1.073800	1.1099
14	$3s^24p(^2P^o)$	1/2	1.288321	1.3487
15	$3s^24p(^2P^o)$	3/2	1.289567	1.3496
16	$3p^3(^2D^o)$	3/2	1.342508	1.3864
17	$3p^3(^2D^o)$	5/2	1.343073	1.3868
18	$3p^3(^4S^o)$	3/2	1.455433	1.4907

The total wave function of  $P^+$  included  $0 \leq \ell \leq 10$  partial waves for the interacting electron and 16 continuum functions for the  $R$ -matrix basis sets. The  $R$ -matrix boundary was chosen to be large enough, 15  $a_0$ , to accommodate the bound orbitals. The second term of the

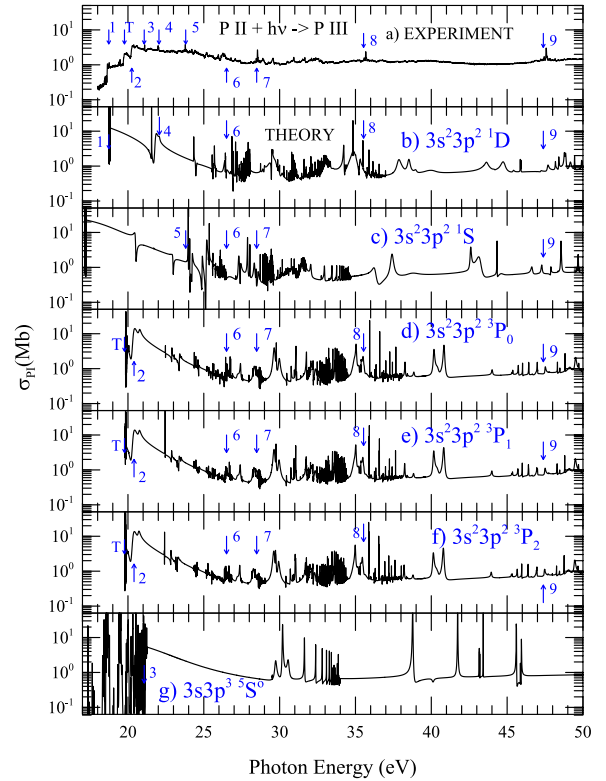


**Fig. 2.** Comparison of photoionization cross sections  $\sigma_{PI}$  of P II between the measured spectrum (panel (a)) and predicted values from six individual levels  $3s^23p^2(^3P_{0,1,2}, ^1D_2, ^1S_0)$  and  $3s3p^3(^5S^o)$  (panels (b)–(g)). A number of resonant structures, numbered from 1 to 9, in panel (a) are being identified with those in panels (b)–(g). “T” denotes the threshold energy for the ground state. All panels correspond to the same vertical scale except the top one.

wave function, which represents the bound state correlation functions, included 39  $(N+1)$ -particle configurations with orbital occupancies from minimum to a maximum number as given within parentheses of the orbitals  $1s(2-2)$ ,  $2s(2-2)$ ,  $2p(6-6)$ ,  $3s(0-2)$ ,  $3p(0-4)$ ,  $3d(0-3)$ ,  $4s(0-2)$ ,  $4p(0-2)$ ,  $4d(0-2)$ ,  $4f(0-1)$ , and  $5s(0-1)$ .

Photoionization cross sections are obtained with consideration of radiation damping for all bound levels using the BPRM  $R$ -matrix codes [15–17]. The narrow resonances of photoionization were delineated at a very fine energy mesh.

## 5. Results and discussions

The experimental results for  $\sigma_{PI}$  are presented in Fig. 1 and, in the first panels of Figs. 2–4. The measured data points in the spectrum of Fig. 1 are plotted with black dots joined by a gray line that can be noticed only in the peaks due to the high density of the data. This spectrum was normalized to  $\sigma_{PI}$  absolute measurements of Table 2. These cross sections were measured at energy values where the spectrum appears to be structureless. To perform the normalization, a factor of the cross sections to the ion yield spectrum was derived in the energy values where absolute

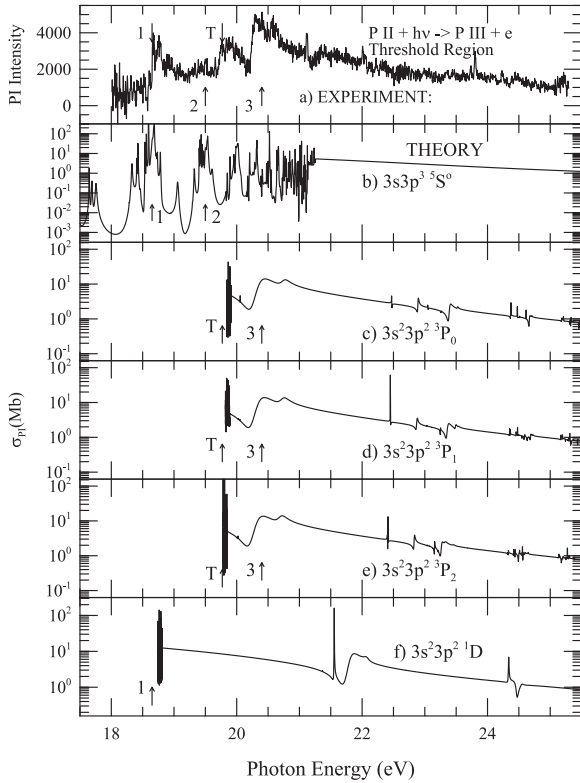


**Fig. 3.** Photoionization cross sections  $\sigma_{PI}$  at and near the thresholds of ground level  $3s^23p^2(^3P_0)$  and a few low lying excited levels  $3s^23p^2(^3P_{1,2})$ ,  $3s^23p^2(^1D_2)$  and  $3s3p^3(^5S_2^o)$  of  $P^+$  illustrating agreement in threshold features (pointed by arrows 1, 2, 3, and T) between the experimental observation (a) and theoretical reproduction in the five individual levels (b)–(f). The letter T indicates the ionization threshold at 19.77 eV (NIST compilation table).

measurements were done. For the spectrum intervals where no absolute values were measured, the normalization factor was derived from a third order spline interpolation.

The  $P^{2+}$  signal of all 1 eV-scans was measured with the interaction region bias-voltage on as a function of the photon energy with the same conditions that were used to measure the absolute cross sections points of Table 2. However, the form factors were not recorded for every point in the 1 eV-scans but monitored to maintain this condition. Hence, the resulting spectrum consisted of a normalized ion-yield spectrum. This ion-yield spectrum was normalized to the cross sections as indicated above.

In Fig. 1, a portion of the spectrum (smaller gray dots joined with a gray line) was multiplied by  $f_c$ . This is the correction function that accounts for high order radiation in the photon beam and is applied below 30 eV. Since we used a rather simplistic approximation for  $f_c$ , we prefer to present both, the corrected and the measured spectrum. A text file with the measured spectrum of Fig. 1 and the correction function  $f_c$  is given in the complementary material section of this publication. To facilitate the comparison with theory, the corrected portion of the

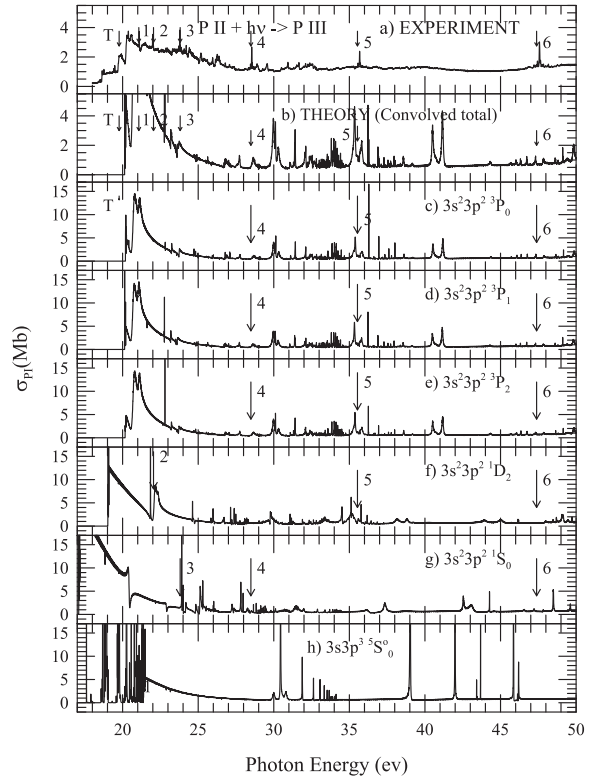


**Fig. 4.** Comparison of single photoionization cross sections  $\sigma_{PI}$  of  $P^+$  between the experiment (panel (a)) and statistically averaged total sum (panel (b)) of cross sections of the six levels,  $3s^23p^2(^3P_{0,1,2}, ^1D_2, ^1S_0)$  and  $3s3p^3(^5S_2^o)$  as presented in panels (c)–(h). The individual cross sections were convolved before the summation. Selected resonant structures (denoted by T, 1–6) are compared in the panels. The averaging has reduced most of the calculated resonances.

**Table 2**

Measured absolute total single photoionization cross section  $\sigma_{PI}$  of  $P^+$  derived from the experimental parameters of Eq. (1). The error corresponds to the quadrature sum of one standard deviation and a systematic uncertainty of 20%. Also the corrected cross section due to a higher order radiation has an additional uncertainty of 50% of the difference between the measured and the corrected cross section (not quoted here).

Photon energy (eV)	$\sigma$ (Mb)	Error (Mb)
19.05	0.62	0.23
27.88	1.02	0.32
30.00	1.00	0.29
40.83	1.21	0.31
48.40	1.36	0.34

experimental spectrum below 30 eV has been inserted in panels (a) of Figs. 2 and 4.

Fig. 1 shows two distinct resonant structures below the ground state ionization limit of  $^3P_0$  at 19.839 eV, indicating contribution from metastable excited states in the initial  $P^+$  ion beam. Based on the observed structures and on the energy range considered, we selected the six lowest levels,  $3s^23p^2(^3P_{0,1,2}, ^1D_2, ^1S_0)$  and  $3s3p^3(^5S_2^o)$  of  $P^+$  for

computation of the photoionization cross sections. We 17 excited levels of the core, presented in Table 1, included in the wave function expansion can give rise to resonances.

We compare the experimentally observed features of  $P^+$  photoionization with the theoretical predictions in Fig. 2. For identification of features we plot the theoretical  $\sigma_{PI}$  of each of the six lower levels in panels (b)–(g), panel (a) presents the experimental results. The ionization threshold for the ground state  $^3P$  is indicated by notation ‘T’ in panels (a) and panels (d)–(f).

A number of common features between the experiment and predicted cross sections can be identified in Fig. 2. To compare, we have selected some features, numbered from 1 to 9, in the measured spectrum (a) and show their corresponding feature in the individual theoretical  $\sigma_{PI}$  in panels (b)–(g) of Fig. 2.

Photoionization of fine structure levels  $3p^2(^3P_{0,1,2}, ^1D_2, ^1S)$  of the ground configuration of  $P^+$  in panels (b)–(f) in Fig. 2 show characteristic features, such as, a narrow resonance at threshold T and a prominent broad resonant structure beyond it. Electron–ion recombination, which is the inverse process of photoionization, increases with increase of the latter. Hence these high peak resonances indicate higher recombination rate of  $P^+$  particularly at low temperature where contribution to recombination comes mainly from low energy, that is, near threshold region. The broad structure is similar to that in the photoionization of  $^3P$  ground state of Si (Fig. 1 in Nahar and Pradhan [4]) which has the maximum similarity to  $P^+$  because it is isoelectronic to and the preceding element to phosphorus in the periodic table. Calculation for Si was carried out in non-relativistic LS coupling and did not find the narrow resonance at the threshold. Inclusion of relativistic effect in the present work has split the ionization energy in to three levels  $^3P_{0,1,2}$  via fine structure and the couplings of fine structure channels have introduced the important sharp resonance right at the thresholds not seen for Si. The broad feature arises by the summed combination of autoionizing resonant states that belong to the Rydberg series of states  $3s3p^2(^4P)\nu l(^3S^o, ^3P^o, ^3D^o)$  converging on to excited core state  $3s3p^2(^4P)$  and are allowed by the ground state  $3s^23p^2(^3P)$ .

For the low charged  $P^+$  ion, relativistic effects included through BPRM method, may not have significant effect on the calculated  $\sigma_{PI}$  for most of the energy range. Nevertheless, the resonances often are introduced at and near threshold region by couplings of fine structure channels (e.g., [11,21]), not allowed in LS coupling, naturally exist as seen in this experiment. For  $P^+$ , they form from allowed autoionizing fine structure channels  $2p(^2P_{3/2}^o)\nu s_{1/2}$  and  $2p(^2P_{3/2}^o)\nu d_{3/2,5/2}$  to give  $^3S_1^o, ^3P_1^o, ^3D_1^o$  levels. Comparison of the present  $\sigma_{PI}$  of the other excited level of the ground configuration, such as  $^1D_2$ , to that of Si also shows similar features and additional resonances at-threshold due to couplings of fine structure channels.

Consideration of the relativistic effect has another important effect in the resonances of the  $3s3p^3(^5S_2^o)$  level. In contrast to  $^3P$  levels, this level does not couple to the core ground state  $^2P^o$ . The ionization energy for the level is 1.06 Ry (14.11 eV) and its first ionized state is  $3s3p^2(^4P)$ , which is approximately at an energy of 0.515 Ry (7.1 eV). Hence  $\sigma_{PI}$  is not expected to show up below 21.2 eV (14.11 + 7.1 eV) in non-relativistic LS coupling. However, in reality the state is photoionized at the ionization threshold 14.11 eV and this can only be explained by consideration of relativistic effects as seen in panel (g). Although the background cross section is almost zero, that is, a weak continuum below 21.2 eV, the energy region is filled with extensive resonances with high peaks. They are appearing from relativistic fine structure couplings, as explained in a similar case for  $C^{2+}$  [21]. The enhancement at 21.2 eV is visible as resonant structure 3 in panel (a) of Fig. 2.

The resonances below 21.2 eV of  $3s3p^3(^5S_2^o)$  level in Fig. 2(g) are seen clearly in panel (b) of Fig. 3. The pattern of resonances indicates quite a number of series of configurations  $3s3p^2(^4P)\epsilon s$  and  $3s3p^2(^4P)\epsilon d$  where  $\epsilon$  represents continuum. Through fine structure  $j=2$  level of  $^5S_2^o$  is allowed to photoionize to  $J=1,2,3$  levels of even parity. They can arise from 3 such  $J\pi$  channels of  $3s3p^2(^4P)\epsilon s(^5P_{1,2,3})$ , 9 channels of  $3s3p^2(^4P)\epsilon d(^5P_{1,2,3}, ^5D_{1,2,3}, ^5F_{1,2,3})$  and 6 channels of  $3s3p^2(^4P)\epsilon d(^3P_{1,2}, ^3D_{1,2,3}, ^3F_{2,3})$ . In other words the resonant complex below 21.2 eV is composed of 18 overlapping series of Rydberg resonances. Some of the series, particularly with  $\epsilon d$ , are expected to be more prominent than the others. Only when few series are present it is possible to identify them spectroscopically using quantum defect analysis, what could be used for some diagnostics, but this is unfortunately not the case here.

Comparison between panel (a) and panels (b)–(g) in Fig. 2 show that peak 3 arises from  $^5S_2^o$  level, peak 4 is from  $^1D_2$  level, and peak 5 from  $^1S_0$  level. Although the high base-line of  $^1S$  is missing below threshold T of measured spectrum, a couple of its peaks still appear to coincide with those in panel (a). In fact,  $^1S_0$  contribution can be expected to be low due to its small statistical weight factor (as will be seen in the convolved spectrum in Fig. 4). Resonant structures 6 and 7 of panel (a) in Fig. 2 can have combined origination from a number of levels, such as,  $^3P_{0,1,2}$ , and additional level  $^1S$  for peak 7. Similarly peak 8 arises from  $^3P_{0,1,2}$  and  $^1D$ .

However, resonant structure labeled as 9 in the observed spectrum is more prominent than the weaker resonances appearing at the same energy position in calculated  $\sigma_{PI}$  of  $^3P_{0,1,2}$  and  $^1S$ . Hence, this particular structure 9 may have contribution from an additional unaccounted excited state of  $P^+$ . It may belong to a long living state, such as,  $3s^23p^2P^o3d(^3F^o)$ . The time of flight of 6 keV  $P^+$  ions for the 4.9 m distance from the ECR ion source to the center of the interaction region is 25  $\mu s$ . It may be that peak labeled as 5 at 23.78 eV could be a replica of peak

labeled as 9 at 47.58 eV caused by second order radiation in the photon beam. Except this, comparison gives clear evidence of dominant contributions to the cross section from six low lying levels of  $P^+$ :  $3s^23p^2(^3P_{0,1,2}, ^1D_2, ^1S_0)$  and  $3s3p^3(^5S_2^o)$ .

Calculated cross sections show more resonances than the measurement. These resonances are quenched by the physical conditions in the experiment, such as, population of one state can be higher than others, spectral width of the photon beam etc.

For the purpose of verification and because of its relevance, the threshold region was remeasured in an independent experimental campaign with the same apparatus by means of spectroscopic ion-yield but with a slightly higher photon energy resolution of 20 meV. The measured threshold-spectrum is shown in panel (a) of Fig. 3. Also, an independent gas-cell energy calibration was carried out. The lower panels (b)–(f) in Fig. 3 show, in more detail,  $\sigma_{pl}$  contributions of the five levels from the present ab initio  $R$ -matrix calculations (scales in the plot are chosen for the best illustration of features). It is easier to distinguish some structures than in Fig. 2. Features denoted by 1, 2, 3 and  $T$  in (a) are pointed by arrows along the panels to identify with those in calculated BPRM  $\sigma_{pl}$  for the ground  $3s^23p^2(^3P_0)$  and a few low lying excited levels  $3s^23p^2(^3P_{1,2}, ^1D_2)$  and  $3s3p^3(^5S_2^o)$  of  $P^+$ . The resonant structures at 1 and  $T$  in the experimental spectrum (panel (a) in Fig. 3) show agreement with those at thresholds of individual levels  $3s^23p^2(^3P_{0,1,2}, ^1D_2)$ . The structures marked by 2 and 3 match with those of  $3s^23p^2(^3P_{0,1,2})$  and  $3s3p^3(^5S_2^o)$ . The structure below 1 (panel (a) in Fig. 3) is largely due to  $3s3p^3(^5S_2^o)$  (panel b). Existence of the same features both in experiment and theory, Figs. 2 and 3, confirm the composition of levels in the ion beam and hence benchmark the features with both the experiment and BPRM theory.

Reproduction of observed structures in the present calculations determined the existing initial states of  $P^+$  in the ion beam. However, measured strengths of resonant structures depend on the photon energy resolution and on their natural width. The background cross section depends largely on the population of states in the ion beam. These factors introduce differences in magnitude and in sharpness in features between the experimental and theoretical spectra. In order to produce a total spectrum of the six levels considered for a general comparison with the experimental spectrum, we summed the individual cross sections statistically as

$$\langle \sigma_{pl} \rangle = \sum_k \left[ \frac{\sum_i (2J_i + 1) \sigma_{pl}^k(i)}{\sum_i (2J_i + 1)} \right], \quad (8)$$

where sum over  $k$  is for all six levels of  $P^+$ . Before carrying out the sum, we convolved  $\sigma_{pl}$  of each level,  $3s^23p^2(^3P_{0,1,2}, ^1D_2, ^1S_0)$  and  $3s3p^3(^5S_2^o)$ , with a Gaussian profile of width 10 meV which is narrower than the actual

experimental resolution (24 meV in Fig. 1) to avoid dissolution of sharp features. This retained the features specific to the levels for identification purpose. Gaussian convolution of the calculated cross section to simulate the spectral resolution of the experiment has been successful in reproducing photoionization features for  $C^+$  [21],  $O^+$  [7] and  $O^{q+}$  with  $q=2,3,4$  [22].

The convolved cross sections of the six levels and the statistical sum of them are presented and compared with experiment in Fig. 4. While the total  $\sigma_{pl}$ , panels (a) and (b), are plotted with the same scale, the individual ones – panels (c)–(h) – have different scales to show their features. A number of features (pointed by arrows and denoted by  $T$ , 1–6) of Fig. 2 have been arbitrarily selected to illustrate the effect of the convolution and the statistical sum. We note that the convolution has shrank the resonances of each level significantly and dissolved a good fraction of them. The exception is the predicted broad feature in  $\sigma_{pl}$  in the threshold region beyond  $T$  which is much higher than the measured value which was raised some by after application of the correction  $f_c$ . Comparison of the total spectra in panels (a) and (b) in Fig. 4 show that while some features have remained, the statistical summation has also dissipated, to different extents, a number of resonances. For example, the threshold rise in  $^1S$  is significantly diminished. This could be expected due to low statistical weight factor. The differences can be explained with several reasons. The calculated resonances are narrow due to fine structure splitting and hence can be reduced during averaging. Some effect can also be from the spectral resolution, as described in the experiment section. The experimental spectra consist of quantum contributions from the ground as well as from low lying states convoluted by the spectral resolution of the experiment.

Previous experimental evidence in C-like ions [22] shows that populations of the  $^5S_2^o$  excited level are one order of magnitude below the population given by Eq. (8) which is likely to overestimate its actual population. However, as stated before, the goal of the present work is to prove the present first-principles derived theoretical approach.

The background cross section of measured spectrum is higher than the predicted spectrum from statistical sum. Percentage of population of the states in the ion beam can change background as found, such as for  $O^+$  photoionization [7]. Metastable initial states in the  $P^+$  ion beam are, at least in principle, produced by collisions with energetic electrons in the ECR ion source. In addition to collisions with electrons, secondary resonant collisions with the residual gas may quench [23,24] with unknown efficiencies, some of the electronic excitation. In general, processes inside the ion source generate an undetermined amount of metastable component in the ion beam. Hence, trials with arbitrary percentages of populated states may eventually result in a combined theoretical spectrum that will agree better with the measured spectrum. For less complex systems such as  $C^+$  [21], where Rydberg series of resonances do not overlap as extensively as in  $P^+$  and where the population fractions are known, a better

agreement can be achieved. However, this is not the objective of the present work. Instead, we focused on benchmarking observed features and structure in the photoionization spectra by comparing with theoretical calculations.

## 6. Conclusions

We report a study of the single photoionization of phosphorus cation  $P^+$ . The study was conducted in the photon energy range of 18 eV (68.9 nm) to 50 eV (24.8 nm). Experiment was performed by means of the merged beams technique and calculation was carried out in ab initio relativistic Breit–Pauli  $R$ -matrix (BPRM) method. The present theoretically predicted results have been able to reproduce the main features in  $\sigma_{PI}$  of  $P^+$  seen in the experimentally measured spectrum.

The photon energy resolution for the experiment was 24 meV. We found features in the measured photoionization spectrum that can be explained as mainly originated from the ground state and the five lower lying excited levels of this highly reactive element. Photoionization cross sections ( $\sigma_{PI}$ ) of the ground state exhibits high peak resonances and considerably enhanced background in the low energy region starting at the ionization threshold (about 20 eV).

A slowly decaying background of  $\sigma_{PI}$  at the higher energy region of the spectrum show the existence of identifiable resonant features of six low lying levels. Features, particularly at and near threshold, form due to couplings of relativistic fine structure levels. These coupling effects are not allowed in non-relativistic LS coupling approximation that was previously used for  $\sigma_{PI}$  calculation of Si. This proves importance of relativistic fine structure effects in low energy which is typically ignored for low charge mid-size ions.

Finally, we studied the effect of statistical addition of the calculated cross sections of the six levels convolved with a Gaussian function for a combined total cross sections spectrum. We note that most of the resonant features diminished in the convolved spectrum as a consequence of very narrow resonance structures that lay very close and intermingle with each other. The overall cross section intensity agreement and structures identifications show good agreement of the theory with the experiment. Hence, the present results should facilitate more accurate modeling of  $P^+$  for practical applications.

All photoionization data are available electronically from NORAD-Atomic-Data (NaharOSURadiativeAtomicData) at website: <http://norad.astronomy.ohio-state.edu>.

## Acknowledgments

The Advanced Light Source is supported by the Director, Office of Science, Office of Basic Energy Sciences, of the U.S. DOE Contract DE-AC02-05CH11231. S.N. Nahar acknowledges partial support from NSF grant AST-1312441 and DOE grant DE-SC0012331. The computational work was carried out at the Ohio Supercomputer Center in

Columbus Ohio. A.M.C. and K.C.C. acknowledge the US DOE NNSA through Cooperative Agreement DE-FC52-06NA27616. The US National Science Foundation. D.H. acknowledges support from the Swedish Research Council. A.M.J. acknowledges support from CONACyT grant CB-2011-01 167631. G.H., E.M.H., L.H. and A.A. acknowledge grant UNAM IN106915. G.H. acknowledges a DGAPA-PASPA sabbatical scholarship. The authors acknowledge Ulises Amaya and Reyes García computational support.

## References

- [1] Koo B-C, Lee Y-H, Moon D-S, Yoon S-C, Raymond JC. Phosphorus in the young Supernova remnant Cassiopeia a. *Science* 2013;342(6164):1346–8. <http://dx.doi.org/10.1126/science.1243823> [URL (<http://www.sciencemag.org/content/342/6164/1346.abstract>)].
- [2] Team TOP. The opacity project, vols. 1 and 2; 1996.
- [3] Mendoza C, Zeppen CJ. Photoionisation cross sections of the ground states of neutral Si, P and S. *J Phys B* 1988;21:259–66. <http://dx.doi.org/10.1088/0953-4075/21/2/010> [URL (<http://iopscience.iop.org/0953-4075/21/2/010>)].
- [4] Nahar SN, Pradhan AK. Atomic data for opacity calculations: XVIII. Photoionization and oscillator strengths of Si-like ions  $Si^0$ ,  $Si^{2+}$ ,  $Ar^{4+}$ ,  $Ca^{6+}$ . *J Phys B* 1993;26:1109–27.
- [5] Nahar SN. Electron recombination rate coefficients and photoionization cross sections for astrophysically abundant elements. III. Si-sequence ions: Si I, S III, Ar V, Ca VII, and Fe XIII. *Astrophys J Suppl Ser* 2000;126:537–50.
- [6] Phaneuf RA, Havener CC, Dunn GH, Müller A. Merged-beams experiments in atomic and molecular physics. *Rep Prog Phys* 1999;62(7):1143 [URL (<http://stacks.iop.org/0034-4885/62/i=7/a=202>)].
- [7] Covington AM, Aguilar A, Covington IR, Gharaiabeh MF, Hinojosa G, Shirley CA, et al. Photoionization of  $Ne^+$  using synchrotron radiation. *Phys Rev A* 2002;66:062710. <http://dx.doi.org/10.1103/PhysRevA.66.062710>.
- [8] Müller A, Schippers S, Hellhund J, Holste K, Kilcoyne ALD, Phaneuf RA, et al. Single-photon single ionization of  $W^+$  ions: experiment and theory. *J Phys B* 2015;48(23):235203 [URL (<http://stacks.iop.org/0953-4075/48/i=23/a=235203>)].
- [9] Domke M, Schulz K, Remmers G, Kaindl G, Wintgen D. High-resolution study of  $1^1P^o$  double-excitation states in helium. *Phys Rev A* 1996;53:1424–38. <http://dx.doi.org/10.1103/PhysRevA.53.1424> [URL (<http://link.aps.org/doi/10.1103/PhysRevA.53.1424>)].
- [10] King GC, Tronc M, Read FH, Bradford RC. An investigation of the structure near the  $L_{2,3}$  edges of argon, the  $M_{4,5}$  edges of krypton and the  $N_{4,5}$  edges of xenon, using electron impact with high resolution. *J Phys B* 1977;10:2479–95.
- [11] Pradhan AK, Nahar SSN. Atomic astrophysics and spectroscopy. New York; Cambridge: Cambridge University Press; 2011.
- [12] Burke P, Robb W. The  $R$ -matrix theory of atomic processes. *Adv Atom Mol Phys* 1976;11:143–214.
- [13] Seaton MJ. Atomic data for opacity calculations. I. General description. *J Phys B* 1987;20(23):6363 [URL (<http://stacks.iop.org/0022-3700/20/i=23/a=026>)].
- [14] Berrington KA, Burke PG, Butler K, Seaton MJ, Storey PJ, Taylor KT, et al. Atomic data for opacity calculations. II. Computational methods. *J Phys B* 1987;20:6379 [URL (<http://stacks.iop.org/0022-3700/20/i=23/a=027>)].
- [15] Berrington KA, Eissner WB, Norrington PH. RMATRIX1: Belfast atomic  $R$ -matrix codes. *Comput Phys Commun* 1995;92:290–420. [http://dx.doi.org/10.1016/0010-4655\(95\)00123-8](http://dx.doi.org/10.1016/0010-4655(95)00123-8) [URL (<http://www.sciencedirect.com/science/article/pii/0010465595001238>)].
- [16] Nahar SN, Pradhan AK. Unified treatment of electron-ion recombination in the close-coupling approximation. *Phys Rev A* 1994;49:1816–35. <http://dx.doi.org/10.1103/PhysRevA.49.1816> [URL (<http://link.aps.org/doi/10.1103/PhysRevA.49.1816>)].
- [17] Zhang HL, Nahar SN, Pradhan AK. Close-coupling  $R$ -matrix calculations for electron-ion recombination cross sections. *J Phys B* 1999;32(6):1459 [URL (<http://stacks.iop.org/0953-4075/32/i=6/a=010>)].
- [18] Eissner W, Jones M, Nussbaumer H. Techniques for the calculation of atomic structures and radiative data including relativistic corrections. *Comput Phys Commun* 1974;8:

- 270–306. [http://dx.doi.org/10.1016/0010-4655\(74\)90019-8](http://dx.doi.org/10.1016/0010-4655(74)90019-8) [URL (<http://www.sciencedirect.com/science/article/pii/0010465574900198>)].
- [19] Nahar SN, Eissner W, Chen G-X, Pradhan AK. Atomic data from the Iron project: LIII. Relativistic allowed and forbidden transition probabilities for Fe XVII. *Astron Astrophys* 2003;408: 789–801. <http://dx.doi.org/10.1051/0004-6361:20030945>.
- [20] Kramida A, Ralchenko Yu, Reader J, NIST ASD Team. NIST atomic spectra database (ver. 5.1). Gaithersburg, MD: National Institute of Standards and Technology; 2013. [Online]. Available at: (<http://physics.nist.gov/asd>) [February 25, 2014].
- [21] Nahar SN. Relativistic photoionization cross sections for C II. *Phys Rev A* 2002;65:052702. <http://dx.doi.org/10.1103/PhysRevA.65.052702> [URL (<http://link.aps.org/doi/10.1103/PhysRevA.65.052702>)].
- [22] Champeaux JP, Bizau JM, Cubaynes D, Blancard C, Nahar S, Hitz D, et al. Measurements and calculations of photoionization cross sections of multiply charged ions in ground and metastable states along the isonuclear series of oxygen:  $O^{2+}$  to  $O^{4+}$ . *Astrophys J Suppl Ser* 2003;148: 583–92 [URL (<http://iopscience.iop.org/0067-0049/148/2/583/>)].
- [23] Adams NG, Smith D, Alget E. Reactions of the  $^2P_{3/2}$  and  $^2P_{1/2}$  doublet ground states of  $Kr^+$  and  $Xe^+$  at 300 K. *J Phys B* 1980;13(16): 3235 [URL (<http://stacks.iop.org/0022-3700/13/i=16/a=020>)].
- [24] Ibuki T, Sugita N. Vibrational relaxation of  $CO^+$  ( $A^2\Pi_i, \nu=1$ ) and  $CO^+$  ( $B^2\Sigma^+, \nu=1$ ) ions in the collision with CO molecules. *J Chem Phys* 1983;79:5392. <http://dx.doi.org/10.1063/1.445703> [URL (<http://scitation.aip.org/content/aip/journal/jcp/79/11/10.1063/1.445703>)].